

Motility-induced clustering of active particles under soft confinement

Timo Knippenberg¹, Ashreya Jayaram², Thomas Speck^{2,*} and Clemens Bechinger^{1†}

¹*Fachbereich Physik, Universität Konstanz*

²*Institute for Theoretical Physics IV,
University of Stuttgart, 70569 Stuttgart, Germany*

(Dated: October 26, 2023)

We investigate the structural and dynamic properties of active Brownian particles (APs) confined within a soft annulus-shaped channel. Depending on the strength of the confinement and the Péclet number, we observe a novel re-entrant behavior that is not present in unconfined systems. Our findings are substantiated by numerical simulations and analytical considerations, revealing that this behavior arises from the strong coupling between the Péclet number and the effective confining dimensionality of the APs. Beyond highlighting the important influence of soft boundaries on APs, our research holds significance for future applications of micro-robotic systems.

The spatial confinement of systems typically leads to changes of their physical and chemical properties (melting temperature, band structure, magnetic behavior, etc.) compared to their bulk behavior [1–3]. This also applies to groups of active, i.e. self-propelled, particles (APs), which constitutes the novel class of active matter [4, 5]. Systems composed of APs are distinguished by an intricate interplay between their local density and propulsion speed which gives rise to a motility-induced phase separation (MIPS) [6, 7]. This phenomenon has been observed in a wide range of active systems including synthetic colloidal [8, 9] and bacterial suspensions [10], collectives of ants [11], and has been studied extensively in computer simulations [12–15].

Motivated by the fact that the natural environment of many living APs is dominated by geometrical confinements, e.g. porous media (soils) [16] or narrow blood vessels [17], recent studies have investigated their properties near surfaces [18, 19], within channels [20], and confined to optical traps [21]. These studies demonstrate that spatial confinement has a pronounced influence on the behavior of APs promoting, e.g. the formation of lanes and bands [22]. Such confinement-induced behavior is also important in view of potential applications of synthetic APs such as embolization [17] or drug delivery [23]. Opposed to extensive work on APs in bulk and near *hard* walls and channels, however, only few studies have investigated the behavior of APs confined by *soft* boundaries where the effective confinement strongly depends on the propulsion velocity v . Because MIPS has been demonstrated to be largely suppressed [24, 25] for one-dimensional (1D) confinements (opposed to higher dimensions [12, 26–28]), this suggests a non-trivial phase behavior of APs in soft confinements as a function of their propulsion velocity.

In this Letter, we experimentally and numerically study the clustering of APs in a narrow annular channel created by two concentric soft repulsive barriers. By

varying the softness of these barriers and the velocity v of the APs, we can systematically tune the effective dimensionality of the system from one (single-file) to two spatial dimensions (2D). Upon increasing the AP propulsion velocity or the softness of the confinement, we find a transition from a homogeneous to an inhomogeneous cluster phase and eventually back to a homogeneous AP distribution within the annulus. Such re-entrant behavior is a unique feature of soft confinements and finds no resemblance in 2D systems where phase separation persists for all activities above the critical point.

In our experiments, we use N active Janus particles composed of silica spheres (diameter $\sigma = 7.8 \mu\text{m}$) coated with a 60 nm thick carbon layer on one hemisphere. Due to gravitational and hydrodynamic forces, their motion is restricted to the lower bottom of the sample cell. When suspended in a critical binary mixture of water and propylene-glycol-n-propyl ether (PnP) (40 %m) and illuminated with a laser beam ($\lambda = 532 \text{ nm}$), the carbon caps are selectively heated. This leads to an asymmetric demixing of the fluid around the particle [29, 30]. As a result, the particles perform an active Brownian motion whose propulsion velocity v is controlled by the laser intensity. In our experiments we use a single laser beam which is permanently scanned over all APs and focused on their carbon cap. In the following, we use the Péclet number $\text{Pe} \equiv 3v/(D_R\sigma)$ to characterize v with the rotational diffusion coefficient $D_R \approx 0.00125 \text{ s}^{-1}$, see Supplemental Material (SM) [31].

To create barriers with adjustable softness, we use an additional stationary laser pattern consisting of two concentric rings with mean radius $R = 55 \mu\text{m}$ and gap width $g = 2 \mu\text{m}$ (see in Fig. 1(a)). When APs approach these rings, the intensity gradient modifies the shape of the demixing regions around APs and thus re-orientates the direction of AP propulsion relative to their orientation [32]. This repulsion from an increasing light gradient leads to an effective external potential $V(r)$ (Fig. 1(b)) acting on the APs. The confining strength is controlled by the intensity of the concentric laser pattern [33, 34]. In contrast to a topographical confinement, this approach avoids the influence of hydrodynamic interactions with the boundaries.

* thomas.speck@itp4.uni-stuttgart.de

† clemens.bechinger@uni-konstanz.de

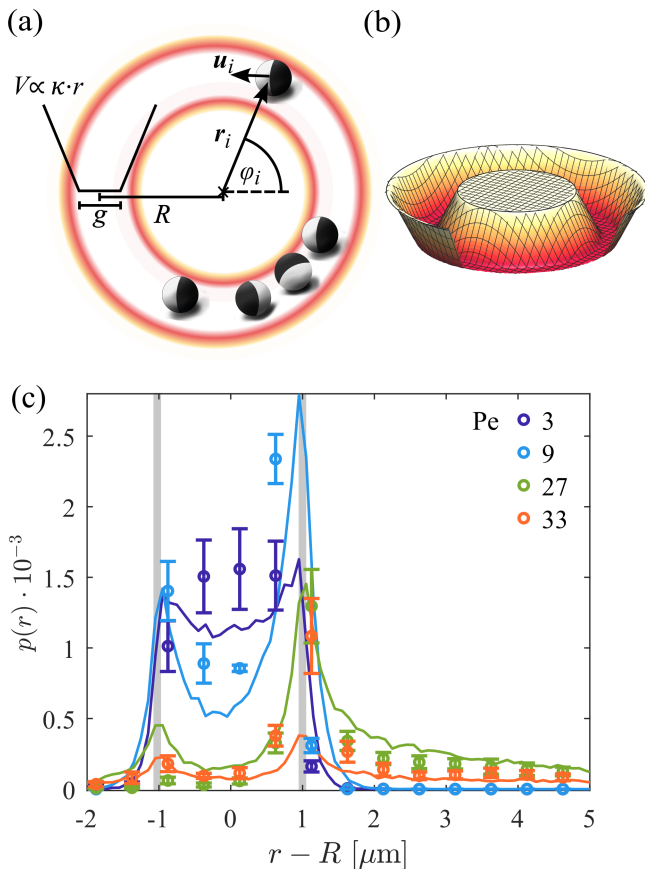


FIG. 1. (a) Schematic view of APs confined to an annular-shaped confinement, the latter providing an effective potential as shown in (b). (c) Radial position probability density $p(r)$ of a single AP inside the confinement for different Pe and a confinement strength $\kappa = 70 \frac{k_B T}{\sigma}$. Circles refer to experimental data, while lines show the corresponding curves from simulations. The gray vertical lines indicate the position of the soft confining walls at $r = R \pm \frac{g}{2}$.

To experimentally demonstrate the creation of adjustable soft confinements, we determined the radial density $p(r)$ of a single AP as a function of Pe and the confinement strength κ , the latter being quantified further below (Fig. 1(b) and SM). At fixed $\kappa = 70 \frac{k_B T}{\sigma}$ and Pe = 3, $p(r)$ peaks around $r = R$. For larger Pe the APs are able to increasingly move towards the repulsive barriers which leads to an increasing width of $p(r)$. In addition, two maxima at $r \approx R \pm 1 \mu\text{m}$ appear. They result from the AP accumulation at the inner and outer soft boundary, similar to what is known for their behavior near hard walls [18, 35, 36]. Moreover, as Pe grows, $p(r)$ becomes highly asymmetric with a tail towards the outer confinement. This is due to the preference of APs to accumulate at concave rather than convex boundaries [37, 38]. A comparable behavior is observed when Pe is fixed and κ is varied (see SM).

In addition to experiments, we also performed numerical simulations where APs are modeled as active Brown-

ian particles moving in 2D. The dynamics of the position \mathbf{r}_i and orientation ϑ_i of the i th AP is governed by

$$\dot{\mathbf{r}}_i = v\mathbf{u}_i + \frac{D_T}{k_B T} (-\nabla V_{\text{WCA}} + \mathbf{f}_i) + \sqrt{2D_T}\zeta_{T,i} \quad (1)$$

$$\dot{\vartheta}_i = M \sum_{j \in \Omega_i} \sin[2(\vartheta_j - \vartheta_i)] \Pi(\vartheta_i, \vartheta_j) + \sqrt{2D_R}\zeta_{R,i}, \quad (2)$$

where unit orientation vector $\mathbf{u}_i \equiv (\cos \vartheta_i, \sin \vartheta_i)^T$ and D_T is the translational diffusion constant. The components of $\zeta_{T,i}$ and $\zeta_{R,i}$ are obtained from a unit normal distribution. The APs interact via the repulsive short-range Weeks-Chandler-Anderson (WCA) potential V_{WCA} [39] modeling volume exclusion. Going beyond the standard model of active Brownian particles, we anticipate lubrication effects to play a major role in a strongly confined system. Previous works on squirmers [40, 41] and Quincke rollers [42] indicate that these interactions prompt an effective alignment between APs. To account for this, we additionally impose an aligning torque of strength M . We find that a choice of $M = 10^4 D_R$ results in good agreement between simulations and experiments as discussed below. The indicator function $\Pi(\vartheta_i, \vartheta_j)$ is unity if the relative orientation of the two APs is between $\pi/2$ and $3\pi/2$ and zero otherwise. The total torque on the i th AP is then the sum over all pairwise torques exerted due to neighboring particles within a circular region Ω of radius $2^{1/6}\sigma$ centered at \mathbf{r}_i . We model the confining force on the i th AP as

$$\mathbf{f}_i = \begin{cases} \kappa \mathbf{e}_{r,i} & \text{if } |\mathbf{r}_i| < (R - \frac{g}{2}) \\ -\kappa \mathbf{e}_{r,i} & \text{if } |\mathbf{r}_i| > (R + \frac{g}{2}) \\ 0 & \text{otherwise} \end{cases} \quad (3)$$

with $\mathbf{e}_{r,i} \equiv (\cos \varphi_i, \sin \varphi_i)^T$ the normal vector. To validate the assumption of a constant force to emulate the confinement, we calculate the density distribution $p(r)$ of a single AP along the radial direction obtained from simulations. As shown in Fig. 1(c), the distributions agree well with experiments. At large κ , however, we observe deviations due to the propulsive force being much weaker than the confining force (for further details, see SM [31]).

The interplay of confinement and self-propulsion determines the phase behavior of APs. Representative snapshots of the steady state for $\kappa = 110 \frac{k_B T}{\sigma}$ and different Pe are shown in Fig. 2(a)-(c) and are obtained for $N = 30$. To quantify the particle density, we introduce the filling fraction $\phi \equiv N\sigma/(2\pi R)$, which yields for our experimental conditions $\phi \simeq 0.68$. At Pe = 3, APs are effectively confined to 1D (single file conditions) with only little radial fluctuations. Particles organize into chains which permanently break up into fragments and reform (supplementary videos 1 and 2). Such behavior is in good agreement with previous studies that confirm the absence of macroscopic phase separation of APs in 1D channels [24]. Upon increasing Pe to Pe = 27, APs are able to pass each other and form multi-layered, dense dynamical clusters which coexist with a surrounding gas

phase (supplementary video 3). For the conditions shown here, these clusters are comprised of typically more than half of the APs and they are stable over timescales of several D_R^{-1} . Such behavior is comparable to MIPS in 2D systems. Note, however, the phase separation in our experiments is observed for smaller Pe compared to 2D systems, where at least $Pe \gtrsim 40$ [26]. At the largest Pe achieved in our study ($Pe = 33$), the radial fluctuations of APs further increase which reduces their effective density (supplementary video 4). Similar to 2D systems where MIPS is absent at low densities, also in our case the clusters disappear and the system becomes more homogeneous in angular direction.

To quantify the Pe-dependent changes of the AP behavior, we perform a Voronoi tessellation. We restrict the evaluation to an annulus-shaped area whose inner (R_i) and outer (R_a) radii have been chosen to be sufficiently large to include all APs independent of Pe (here, $L = R_a - R_i = 9.6\sigma$). Fig. 2(d)-(f) show the corresponding Voronoi cells to Fig. 2(a)-(c) where the Voronoi areas A are colored according to their values. The time-averaged (each measurement was averaged over $\approx 36D_R^{-1}$) probability distribution $p(A)$ is shown in Fig. 3. For $Pe = 3$ and 9, $p(A)$ is rather narrow which indicates that APs are homogeneously spread in angular direction within the annulus. With increasing $Pe = 27$, this peak gradually disappears at the expense of a maximum which develops at small A exhibiting a long tail towards larger values. Such behavior indicates the presence of an AP cluster. At the largest $Pe = 33$ the maximum shrinks, leading to a rather more uniform $p(A)$. This corresponds to a random distribution [43] of APs within the annulus (Fig. 2(f)).

Comparable results are also obtained from our numerical simulations. Here the confinement strength κ has

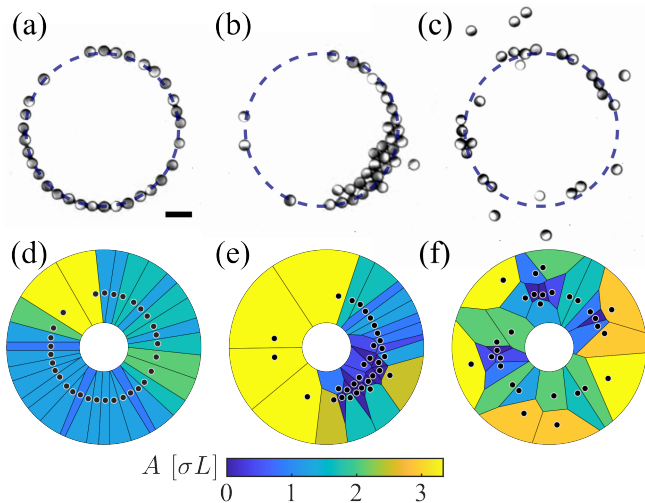


FIG. 2. Representative microscopy images for (a) $Pe = 3$, (b) 27, (c) 33. The scale bar represents $20\ \mu\text{m}$. The dashed lines indicate the channel. (e)-(f) show the corresponding Voronoi tessellations. Colors denote the area A of the Voronoi cells.

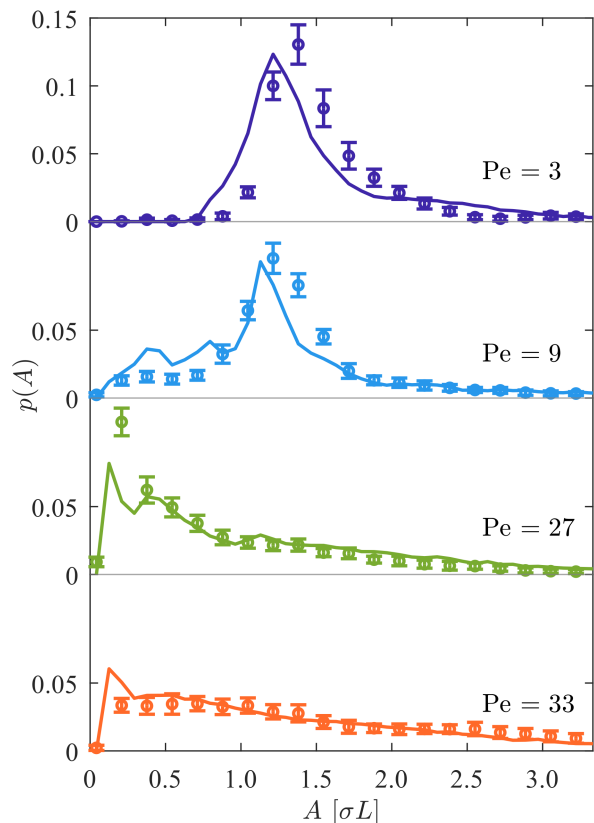


FIG. 3. Probability distribution $p(A)$ of Voronoi cell areas for different Pe and fixed $\kappa = 110k_B T/\sigma$, $N = 30$. Lines represent simulated data, while circles denote experimental data.

been used as a fitting parameter and best agreement to the data previously shown was obtained for $\kappa = 110 \frac{k_B T}{\sigma}$ (solid lines in Fig. 3). The presence of a lubrication-induced torque ($M \neq 0$) is crucial to facilitate the escape of APs in lateral direction upon direct collisions. This promotes the formation of multi-layer clusters in agreement with our experiments.

In Fig. 4, we show the phase diagram of APs in an annular confinement as a function of κ and Pe. As an order parameter to characterize the presence of clusters, we have measured the fraction $\langle N_D/N \rangle$ of APs having a Voronoi area below a threshold value [16]. In our case this threshold was set to be a bit larger than the corresponding value for a 2D closest packing $A < 0.2\sigma L \approx 2\sigma^2$. Clearly, cluster formation is limited to a diagonal region in the κ -Pe space which suggests a re-entrant behavior along both axes. A similar behavior was also found for $N = 46$ ($\phi \simeq 1.04$), i.e. slightly overcrowded systems (SM [31]).

We can rationalize the phase diagram in Fig. 4 from simple geometric considerations. To focus on the essential ingredients, we consider a flat channel confined by perpendicular forces with strength κ . We exploit that for constant force, the density decays exponentially to very

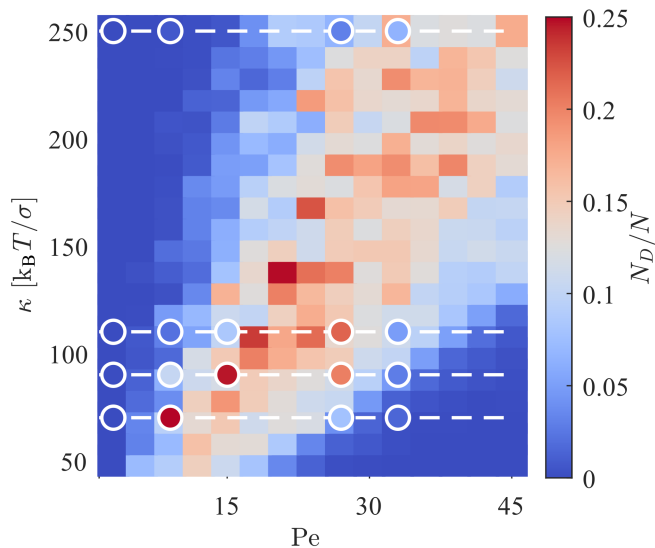


FIG. 4. Phase diagram showing the fraction of APs in a dense surrounding N_D/N for different κ and Pe . Here $N = 30$. The rectangles are simulation data and the circles represent experiments. The dashed lines are guides to the eye.

good approximation [44–46] with sedimentation length

$$\xi = \frac{k_B T}{\kappa} \left(1 + \frac{v^2}{2D_R D_T} \right). \quad (4)$$

This length is reduced as the confining force is increased while APs with larger speed are able to move against the force and to explore a larger area. We model the density distribution as equal to ρ_0 within a stripe of width σ and to decay as $\rho(y) = \rho_0 e^{-|y|/\xi}$ outside. Normalizing the density leads to a dimensionless filling fraction $\phi_0 = \rho_0 \sigma^2 = \phi / [1 + 2\xi/\sigma e^{-\sigma/(2\xi)}]$ within the force-free gap.

Even though in strict 1D only finite clusters form and complete phase separation is preempted [47, 48], the dynamical instability underlying motility-induced phase separation persists. To expose the basic mechanism, we employ the mean-field form [49] of the coexisting filling fractions $\phi_{\pm} = \phi_c \pm \chi \sqrt{v^2 - v_c^2}$ with critical fraction ϕ_c , critical speed v_c , and shape coefficient χ . Figure 5(a) shows these coexisting filling fractions together with ϕ_0 as a function of the sedimentation length ξ . In this representation, ϕ_0 is invariant but ϕ_{\pm} moves to the left as the confining force κ is increased ($\xi_c \sim 1/\kappa$). Above $\kappa > \kappa_{\min}$ both curves cross, defining a range of speeds for which the system becomes inhomogeneous [cf. Fig. 2(b)]. Increasing the speed further, APs overcome the confining force and thus effectively reduce ϕ_0 , returning the system to the active gas phase [cf. Fig. 2(c)]. The resulting phase

diagram in Fig. 5(b) reproduces the salient features of the experiments and simulations, cf. Fig. 4. In particular, there is a range of confining forces κ for which it predicts re-entrant behavior as the speed v is increased

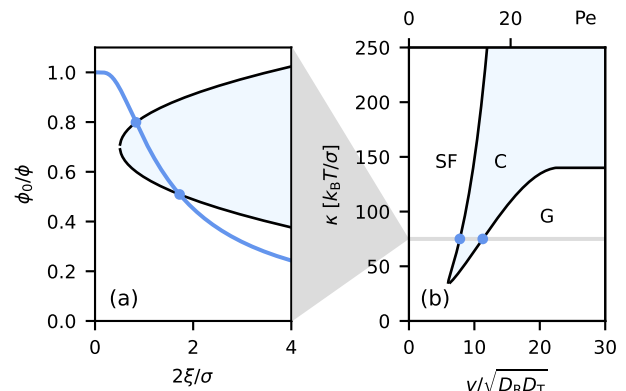


FIG. 5. (a) Filling fraction ϕ_0 (blue line) within a straight confined channel as a function of sedimentation length ξ . Also shown are the coexisting filling fractions ϕ_{\pm} of clusters (black lines) due to the motility-induced instability above the critical speed v_c for $\kappa = 75k_B T/\sigma$. (b) Theoretical phase diagram in the same representation as Fig. 4. The lines delineate the inhomogeneous cluster regime (C) from single file (SF) behavior at small speeds and large forces and the weakly confined homogeneous gas (G). The top axis shows the Péclet number estimated using the measured diffusion coefficients (SM [31]). Parameters are: $v_c = 6\sqrt{D_R D_T}$, $\phi_c = 0.7\phi$, and $\chi = 0.02\sqrt{D_R D_T}\phi$.

in agreement with the experiments. This demonstrates that such re-entrance is a unique property of soft confinements but not found for hard confinements where the accessible area is independent of activity [19, 50, 51].

In summary, we have experimentally studied the clustering of self-propelled colloids in a soft annular-shaped confinement. In agreement with numerical simulations of a minimal model we find that cluster formation is only present in a narrow regime of the confinement strength and the Péclet number, otherwise particles are randomly distributed. This behavior results from a strong coupling of the Péclet number to the radial AP motion which leads to a Pe-dependent change of the effective dimension of the confinement. At low Pe where the APs move in single-file manner, the 1D confinement prevents clustering. At large Pe the increasing radial AP motion reduces the effective particle density which also suppresses clustering (similar to MIPS in two-dimensional systems). Because APs hold great promise as nano-robotic systems, we expect that our study is important in view of how such systems must be operated within soft confinements which are likely to provide realistic conditions in medical applications [17, 23].

-
- [1] F. Varnik and T. Franosch, Non-monotonic effect of confinement on the glass transition, *J Phys Condens Matter* **28**, 133001 (2016).
- [2] K. Nygard, Colloidal diffusion in confined geometries, *Phys Chem Chem Phys* **19**, 23632 (2017).
- [3] A. B. Grommet, M. Feller, and R. Klajn, Chemical reactivity under nanoconfinement, *Nat Nanotechnol* **15**, 256 (2020).
- [4] C. Bechinger, R. D. Leonardo, and H. Löwen et al., Active particles in complex and crowded environments, *Reviews of Modern Physics* **88**, 10.1103/RevModPhys.88.045006 (2016).
- [5] S. Ramaswamy, The mechanics and statistics of active matter, *Annual Review of Condensed Matter Physics* **1**, 323 (2010).
- [6] M. E. Cates and J. Tailleur, Motility-induced phase separation, *Annual Review of Condensed Matter Physics* **6**, 219 (2015).
- [7] Y. Fily and M. C. Marchetti, Athermal phase separation of self-propelled particles with no alignment, *Phys Rev Lett* **108**, 235702 (2012).
- [8] I. Buttinoni, J. Bialke, and F. Kummel et al., Dynamical clustering and phase separation in suspensions of self-propelled colloidal particles, *Phys Rev Lett* **110**, 238301 (2013).
- [9] J. Palacci, S. Sacanna, and S. Steinberg et al., Living crystals of light-activated colloidal surfers, *Science* **339**, 936 (2013).
- [10] G. Liu, A. Patch, and F. Bahar et al., Self-driven phase transitions drive myxococcus xanthus fruiting body formation, *Phys Rev Lett* **122**, 248102 (2019).
- [11] C. Anderson and A. Fernandez-Nieves, Social interactions lead to motility-induced phase separation in fire ants, *Nat Commun* **13**, 6710 (2022).
- [12] A. Wysocki, R. G. Winkler, and G. Gompper, Cooperative motion of active brownian spheres in three-dimensional dense suspensions, *EPL (Europhysics Letters)* **105**, 10.1209/0295-5075/105/48004 (2014).
- [13] J. Stenhammar, D. Marenduzzo, and R. J. Allen et al., Phase behaviour of active brownian particles: the role of dimensionality, *Soft Matter* **10**, 1489 (2014).
- [14] F. Turci and N. B. Wilding, Phase separation and multi-body effects in three-dimensional active brownian particles, *Phys Rev Lett* **126**, 038002 (2021).
- [15] V. Soni, E. S. Bililign, and S. Magkiriadou et al., The odd free surface flows of a colloidal chiral fluid, *Nature Physics* **15**, 1188 (2019).
- [16] F. Moore, J. Russo, and T. B. Liverpool et al., Active brownian particles in random and porous environments, *J Chem Phys* **158**, 104907 (2023).
- [17] J. Law, X. Wang, and M. Luo et al., Microrobotic swarms for selective embolization, *Science Advances* **8**, 10.1126/sciadv.abm5752 (2022).
- [18] J. Elgeti and G. Gompper, Wall accumulation of self-propelled spheres, *EPL (Europhysics Letters)* **101**, 10.1209/0295-5075/101/48003 (2013).
- [19] W. Yan and J. F. Brady, The force on a boundary in active matter, *Journal of Fluid Mechanics* **785**, 10.1017/jfm.2015.621 (2015).
- [20] H. E. Ribeiro and F. Q. Potiguar, Lane formation and crystallization of active matter in a narrow channel, *Physica A: Statistical Mechanics and its Applications* **503**, 849 (2018).
- [21] H. Moyses, J. Palacci, and S. Sacanna et al., Trochoidal trajectories of self-propelled janus particles in a diverging laser beam, *Soft Matter* **12**, 6357 (2016).
- [22] T. Vater, M. Isele, and U. Siems et al., Lane and band formation of oppositely driven colloidal particles in two-dimensional ring geometries, *Phys Rev E* **106**, 024606 (2022).
- [23] L. Abdelmohsen, F. Peng, and Y. Tu et al., Micro- and nano-motors for biomedical applications, *J Mater Chem B* **2**, 2395 (2014).
- [24] P. Dolai, A. Das, and A. Kundu et al., Universal scaling in active single-file dynamics, *Soft Matter* **16**, 7077 (2020).
- [25] I. Mukherjee, A. Raghu, and P. K. Mohanty, Nonexistence of motility induced phase separation transition in one dimension, *SciPost Physics* **14**, 10.21468/SciPostPhys.14.6.165 (2023).
- [26] G. Gonnella, D. Marenduzzo, and A. Suma et al., Motility-induced phase separation and coarsening in active matter, *Comptes Rendus Physique* **16**, 316 (2015).
- [27] A. K. Omar, K. Klymko, and T. GrandPre et al., Phase diagram of active brownian spheres: Crystallization and the metastability of motility-induced phase separation, *Phys Rev Lett* **126**, 188002 (2021).
- [28] A. K. Omar, H. Row, and S. A. Mallory et al., Mechanical theory of nonequilibrium coexistence and motility-induced phase separation, *Proc Natl Acad Sci U S A* **120**, e2219900120 (2023).
- [29] C. Lozano, B. T. Hagen, and H. Lowen et al., Phototaxis of synthetic microswimmers in optical landscapes, *Nat Commun* **7**, 12828 (2016).
- [30] S. Samin and R. van Roij, Self-propulsion mechanism of active janus particles in near-critical binary mixtures, *Phys Rev Lett* **115**, 188305 (2015).
- [31] See Supplemental Material at [URL will be inserted by publisher] for [give brief description of material].
- [32] J. R. Gomez-Solano, S. Samin, and C. Lozano et al., Tuning the motility and directionality of self-propelled colloids, *Sci Rep* **7**, 14891 (2017).
- [33] T. Knippenberg, A. Luders, and C. Lozano et al., Role of cohesion in the flow of active particles through bottlenecks, *Sci Rep* **12**, 11525 (2022).
- [34] Z. Chen, H. Ding, and P. S. Kollipara et al., Synchronous and fully steerable active particle systems for enhanced mimicking of collective motion in nature, *Adv Mater* , e2304759 (2023).
- [35] G. Volpe, I. Buttinoni, and D. Vogt et al., Microswimmers in patterned environments, *Soft Matter* **7**, 10.1039/c1sm05960b (2011).
- [36] G. Li and J. X. Tang, Accumulation of microswimmers near a surface mediated by collision and rotational brownian motion, *Phys Rev Lett* **103**, 078101 (2009).
- [37] Y. Fily, A. Baskaran, and M. F. Hagan, Dynamics and density distribution of strongly confined noninteracting nonaligning self-propelled particles in a nonconvex boundary, *Phys Rev E Stat Nonlin Soft Matter Phys* **91**, 012125 (2015).
- [38] N. Nikola, A. P. Solon, and Y. Kafri et al., Active particles with soft and curved walls: Equation of state, ratchets, and instabilities, *Phys Rev Lett* **117**, 098001 (2016).

- [39] J. D. Weeks, D. Chandler, and H. C. Andersen, Role of repulsive forces in determining the equilibrium structure of simple liquids, *The Journal of Chemical Physics* **54**, 5237 (1971).
- [40] A. Thery, C. C. Maass, and E. Lauga, Hydrodynamic interactions between squirmers near walls: far-field dynamics and near-field cluster stability, *R Soc Open Sci* **10**, 230223 (2023).
- [41] N. Yoshinaga and T. B. Liverpool, Hydrodynamic interactions in dense active suspensions: From polar order to dynamical clusters, *Phys Rev E* **96**, 020603 (2017).
- [42] A. Bricard, J. B. Caussin, and N. Desreumaux et al., Emergence of macroscopic directed motion in populations of motile colloids, *Nature* **503**, 95 (2013).
- [43] M. Tanemura, Statistical distributions of poisson voronoi cells in two and three dimensions, *Forma* **18**, 221 (2003).
- [44] F. Ginot, I. Theurkauff, and D. Levis et al., Nonequilibrium equation of state in suspensions of active colloids, *Physical Review X* **5**, 10.1103/PhysRevX.5.011004 (2015).
- [45] F. Ginot, A. Solon, and Y. Kafri et al., Sedimentation of self-propelled janus colloids: polarization and pressure, *New Journal of Physics* **20**, 10.1088/1367-2630/aae732 (2018).
- [46] S. Hermann and M. Schmidt, Active ideal sedimentation: exact two-dimensional steady states, *Soft Matter* **14**, 1614 (2018).
- [47] J. Tailleur and M. E. Cates, Statistical mechanics of interacting run-and-tumble bacteria, *Phys Rev Lett* **100**, 218103 (2008).
- [48] R. Soto and R. Golestanian, Run-and-tumble dynamics in a crowded environment: persistent exclusion process for swimmers, *Phys Rev E Stat Nonlin Soft Matter Phys* **89**, 012706 (2014).
- [49] T. Speck, A. M. Menzel, and J. Bialke et al., Dynamical mean-field theory and weakly non-linear analysis for the phase separation of active brownian particles, *J Chem Phys* **142**, 224109 (2015).
- [50] A. Duzgun and J. V. Selinger, Active brownian particles near straight or curved walls: Pressure and boundary layers, *Phys Rev E* **97**, 032606 (2018).
- [51] T. Speck and R. L. Jack, Ideal bulk pressure of active brownian particles, *Phys Rev E* **93**, 062605 (2016).
- [52] M. R. Bailey, A. R. Sprenger, and F. Grillo et al., Fitting an active brownian particle's mean-squared displacement with improved parameter estimation, *Phys Rev E* **106**, L052602 (2022).